Alkyl Peroxy Radical Kinetics Measured Using Near-infrared CW−Cavity Ring-down Spectroscopy

Dean B. Atkinson* and Jennifer L. Spillman

Department of Chemistry, Portland State University, Portland, Oregon 97207-0751

Received: March 13, 2002; In Final Form: July 25, 2002

A kinetic reactor system is described which couples pulsed laser photolytic production of radicals with continuous laser excitation cavity ring-down spectroscopic detection in the near-infrared (NIR). The atmospherically relevant alkyl peroxy radicals ethyl peroxy ($C_2H_5O_2$) and methyl peroxy (CH_3O_2) were monitored via their structured absorbance spectra in the NIR near 1.3 μm. These peroxy radicals were then subjected to kinetic study as proof-of-principle for the new technique. Portions of the absorption spectra for the two radicals are reported which agree well with previously published spectra [Hunziker, H. E.; Wendt, H. R. *J. Chem. Phys.* **1976**, *64*, 3488. Pushkarsky, M. B.; Zalyubovsky, S. J.; Miller, T. A. *J. Chem. Phys.* **2000**, *112*, 10695]. The absorption cross sections were determined at selected wavelengths using the known self-reaction rate coefficients and observed kinetic data. The absorption cross sections determined are as follows: for two of the maxima in the origin band of $C_2H_5O_2$, $\sigma_{1317.01\ nm} = \sigma_{1316.40\ nm} = (3.0 \pm 1.5) \times 10^{-21}$ cm^2 molecule^{-1}, and for a maximum in a sequence band of CH_3O_2, $\sigma_{1335.07\ nm} = (1.5 \pm 0.8) \times 10^{-20}$ cm^2 molecule^{-1}. Preliminary data for the prototypical peroxy radical cross-reaction between CH_3O_2 and $C_2H_5O_2$ is presented. This data supports earlier work [Villenave, E.; Lesclaux, R. *J. Phys. Chem.* **1996**, *100*, 14372] which established a pressure independent value of $k(CH_3O_2 + CH_3CH_2O_2) = 2.0 \times 10^{-13}$ cm^3 molecule^{-1} s^{-1} at 298 K. As in most kinetic studies involving peroxy radicals, the accuracy of the reported rate coefficients is influenced by the details of the complex mechanisms used in the fitting. However, in the current studies, specific radical absorption(s) are used to follow each radical's decay, which should improve the precision of the determination.

1. Introduction

Peroxy radicals are key reaction intermediates in the low-temperature oxidation of organic compounds. Alkyl peroxy radicals are important in reaction mechanisms used for understanding and modeling low-temperature combustion, certain industrial processes, and atmospheric chemistry.[1−8] The atmospheric "self-cleansing" mechanism whereby volatile organic compounds (VOCs) are removed from the troposphere features the role of peroxy radicals.[9,10] Peroxy radicals oxidize NO, leading to the production of tropospheric ozone,[11−15] and they are involved in the HO_x (OH and HO_2) cycle.[16] A recent modeling paper speculated that near-infrared photolysis of peroxy radicals could be an important new source of the potent oxidant OH.[17] It has long been acknowledged that uncertainties in the reaction rate coefficients for reactions between peroxy radicals, which vary widely depending on the structure of the peroxy radical, hinder our understanding of the remote troposphere.[18] Despite the importance of peroxy radicals, uncertainties still exist regarding their chemical and photochemical reactivity in the atmosphere; even the thermochemistry of the simplest alkyl peroxy radicals is an area of current study.[19,20] The long-term goal of our research program is to minimize the uncertainties regarding peroxy radical reaction kinetics, especially for the cross-reactions, those between two different peroxy radicals. These studies also will address uncertainties about the near-infrared absorption cross-sections of peroxy radicals. To facilitate these studies, we have constructed a laser photolysis/near-infrared continuous laser excitation cavity ring-down reactor system for the spectroscopic and kinetic study of organic peroxy radicals. The experimental design of the reactor system is described here, as are preliminary results for the prototypical radicals, methyl peroxy (CH_3O_2) and ethyl peroxy ($C_2H_5O_2$). For ease of reference, the standard notation $MeO_2 = CH_3O_2$ and $EtO_2 = C_2H_5O_2$ will be used in place of the names methyl peroxy radical and ethyl peroxy radical, except where the chemical formulas are used.

It has been suggested that the absorption of solar near-infrared radiation (which is not completely attenuated by atmospheric components) by peroxy radicals could lead to photodissociation reactions.[17] One of the suggested reaction pathways leads to formation of hydroxyl radicals, which could have a significant impact on atmospheric chemistry. The modeling of the effect of these suggested photochemical reactions was conducted using several different estimates of the peroxy radical near-infrared absorption cross sections, all of which appear to have been extreme overestimates in light of recent work and our current results.[2,17,21] Investigation of more types of peroxy radicals would be necessary before this suggested mechanism can be discarded. It would also be prudent to consider the possible effects of these photochemical reactions in the laboratory reaction kinetics work, where the flux of the monitoring near-infrared light will be orders of magnitude larger than it is in the atmospheric modeling calculations.

A large fraction of the atmospheric oxidation of VOCs is initiated by hydroxyl radical attack, either by hydrogen abstraction or addition to unsaturated carbons.[5,22] The abstraction reaction is dominant for saturated hydrocarbons, aldehydes, organic acids, and other compounds with labile bonds to

* To whom correspondence should be addressed. E-mail: atkinsond@pdx.edu.

10.1021/jp0257597 CCC: $22.00
Published on Web 08/23/2002

hydrogen, whereas the addition reaction usually dominates for unsaturated compounds and aromatics.[22,23] For hydrocarbons, either type of reaction results in a highly reactive alkyl radical, which under commonly encountered atmospheric conditions (250−300 K, 0.01−1.0 atm pressure, 20% O_2) reacts with molecular oxygen, resulting in nearly immediate formation of an alkyl peroxy radical, generically represented as RO_2.

$$R + O_2 \rightarrow RO_2 \quad (1)$$

The ensuing peroxy radical reaction mechanisms involve some interesting and potentially complex chemistry. The rate coefficients and branching ratios for the reactions of peroxy radicals with NO (which leads to ozone formation),[24−36] with NO_2 (which can form long-lived peroxy nitrates),[25,30,37−39] and with hydroperoxyl, HO_2 (with which all peroxy radicals react rapidly),[30,40−53] are reasonably well established. These reactions are fast and the rate coefficients do not depend strongly on the identity of the peroxy radical. In the remote troposphere (away from the sources of NO and NO_2, collectively known as NO_x), the concentration of NO_x can become low enough that the reactivity of peroxy radicals with themselves or other peroxy radicals and with HO_2 increases in significance. If there are also large emissions of hydrocarbons or other organic compounds by natural sources, the concentration of HO_2 can also be suppressed, in part by the reaction with the other peroxy radicals, resulting in a larger significance of the reactions between peroxy radicals. The extent to which this situation occurs in the remote troposphere has been unclear for some time because of uncertainties in the rate coefficients of the peroxy radical cross-reactions, sometimes referred to as permutation reactions.

The rate coefficients of peroxy radical self-reactions and cross-reactions vary by orders of magnitude depending on which base organic unit (the R in RO_2) is present.[4,6,7] Alkyl peroxy radical cross-reactions primarily involve three product channels, two of which (2b and 2c) lead to stable products (carbonyls and alcohols) that are expected to be removed from the atmosphere more readily by physical (e.g., rainout) and chemical removal mechanisms than the parent hydrocarbon.[3,7,41,54−58]

$$R_1R_2CR_3(\text{e.g., H})O_2 + R_4R_5CR_6(\text{or H})O_2 \rightarrow R_1R_2CR_3(\text{or H})O + R_4R_5CR_6(\text{or H})O + O_2 \quad (2a)$$

$$R_1R_2CHO_2 + R_4R_5CHO_2 \rightarrow R_1R_2CHOH + R_4C(O)R_5 + O_2 \quad (2b)$$

$$\rightarrow R_1C(O)R_2 + R_4R_5CHOH + O_2 \quad (2c)$$

In reaction 2a−c, a more specific generic form (vs RO_2) is used to represent organic peroxy radicals, where the O_2 unit is bonded to a carbon which can also have up to three substituents (R_1−R_6). These may be any molecular fragment from a hydrogen atom to a large organic system. Reaction channels 2b and 2c are only active if one of the substituents is a hydrogen atom (i.e., R_3 and/or R_6 = H) as indicated. This mechanism is also used to characterize the peroxy radical self-reactions, where both radicals are the same and only one of the terminating channels is needed. A fourth energetically possible product channel, the formation of the organic peroxide RO_2R' (analogous to the major product of the $RO_2 + HO_2$ reaction, see below), is not observed,[6,22,59] although the peroxide is probably the activated complex leading to all of the observed channels.[60] Because channel 2a is propagating, whereas reactions 2b and 2c are terminating, the branching ratio α ($\alpha \equiv k_{2a}/(k_{2a} + k_{2b} + k_{2c})$) serves as a measure of the extent to which secondary chemistry will be expected following reaction 2. For tertiary and perhalogenated peroxy radicals such as CF_3O_2, only channel 2a is active ($\alpha = 1$). The radical-propagating channel (2a) produces alkoxy radicals (RO or R_1R_2CHO in reaction 3 below) that react with O_2 if there is an abstractable hydrogen atom on the carbon which is bonded to the oxygen atom.[10,22] This reaction produces a carbonyl and the hydroperoxy radical, HO_2. Hydroperoxy reacts rapidly with peroxy radicals to produce hydroperoxides (RO_2H).[48,49,51,61−69]

$$R_1R_2CHO + O_2 \rightarrow R_1R_2CO + HO_2 \quad (3)$$

$$RO_2 + HO_2 \rightarrow RO_2H + O_2 \quad (4)$$

Larger, more complex alkoxy radicals (RO) can also undergo internal isomerization reactions which sometimes lead to the formation of other peroxy radical products.[70−72] Under atmospheric conditions (and in most laboratory studies), the net effect of reactions 2a, 3, and 4 is to increase the rate of consumption of peroxy radicals beyond what would be expected from reaction 2 alone. Corrections for this effect, which rely on a knowledge of the branching ratio α,[6,7] may be applied in laboratory reaction kinetics to obtain the specific self-reaction rate coefficient (for reaction 2) of interest. However, because of the complexity of the reactive systems, a better strategy is direct modeling/fitting of data to simulations generated with a mechanism containing all of the applicable reactions and absorption cross sections.

The experimental determination of peroxy radical cross-reaction rate coefficients has been challenging.[3,58,68] The fact that both reaction partners are reactive radicals eliminates the possibility of forcing approximate first-order or other simple behavior. The inherent complexity of the secondary chemistry following the reaction of interest implies that complex mechanisms must be used to properly model the kinetic data. Furthermore, there are experimental problems, which can finally be overcome using our new proposed methods. Direct reaction kinetic studies rely upon reliable, sensitive, and time specific detection methods for the radicals of interest. In the case of peroxy radicals, the standard mode of detection has been ultraviolet absorption spectroscopy, and an impressive body of work has been assembled using this methodology.[3,6,7,41,51,54−56,58,62−64,73−79] In these studies, the strong unstructured absorption centered near 240 nm, resulting from the **B** ← **X** electronic transition, is used to monitor peroxy radical concentrations. This method is sensitive (with typical maximum absorption cross sections of 10^{-18} to 10^{-17} cm^2 $molecule^{-1}$)[6,7] and general, because the electronic transition is centered on the −OO moiety.[1,17] Transient absorption spectroscopy coupled with laser photolytic generation of radicals has proven to be an extremely robust kinetic method, especially for the study of the self-reactions.[6,7] Unfortunately, this technique and all others based on UV spectroscopy suffer from a lack of species selectivity among peroxy radicals, because the absorption spectra of many peroxy radicals are similar, with the important exceptions of HO_2 and $CH_3C(O)O_2$.[51,64,75] This lack of species specificity hampers kinetic studies in simple systems and makes the study of more complex systems, like the cross-reactions of interest here, difficult. Promising new approaches for the selective and sensitive time-resolved detection of peroxy radicals for direct kinetics studies include chemical ionization mass spectrometry[80,81] and the near-infrared absorption spectroscopy described here and elsewhere.[2,21]

Because this is our first report of this method, some attention will be given to details of its construction and testing. The heart

of the method is the continuous excitation laser cavity ring-down spectrometer, which has been dubbed CWCRD by others.[82,83] The system reported here is similar to those reported in the literature,[82−84] so a general overview will be given and deviations from the reported construction and operation procedures will be noted and explained. The slow-flow reactor system is of a standard design, so only cursory details will be given. The excimer laser photolysis setup is similar to the long path length design of Yu and Lin,[85] with some important differences which are noted. We believe that this is the first report of the incorporation of a CWCRD spectrometer as the detection component of a slow-flow photolytic kinetic reactor system. Several of the experimental approaches which have been investigated will be described to aid future efforts. The results of proof-of-concept experiments will be presented, including the examination of the cross-reaction kinetics of EtO_2 and MeO_2.

2. Experimental Section

The CWCRD Spectrometer. The cavity ring-down (CRD) technique, using pulsed tunable lasers, has undergone a recent application explosion. Since its introduction in 1988,[86] the appeal of CRD in providing a sensitive variant of absorption spectroscopy has resulted in its application to chemical problems ranging from surface phenomena[87,88] to process measurements in plasmas and flames,[89−103] to atmospheric studies,[104−109] and to a wide range of chemical kinetics studies.[85,98,110−113] Some of the recent applications of CRD spectroscopy and variants of the basic technique are summarized in the chemical literature.[114−117]

The use of continuous laser sources in cavity ring-down was pioneered by Paldus and Zare[84,118,119] and separately by Romanini and co-workers.[82,120] Light is introduced by bringing one of the transmission fringes of the cavity's mode spectrum into resonance with the laser source. The details of the input light coupling vary among the reported CWCRD spectrometers from the highly optimized but experimentally demanding strategy of Paldus[119] to the more easily accomplished but less controllable pseudolocking scheme first advanced by Romanini[82] and used in the system described here. A recent report showed that it is also feasible to bring the light into resonance with the cavity.[121] The excitation light is then rapidly turned off and the ring-down is observed by a photodetector near one of the mirrors. As in the pulsed method, the first-order rate constant of the light intensity decay is equal to the sum of the photon loss processes in the cavity, including mirror-induced transmission, scattering, and absorption, and any scattering and/or absorption processes due to gas (or aerosol) phase species within the cavity. The dimensionless absorbance of the species of interest may be obtained from the difference between the loss rate constant of the ring-down decay for some base condition (no absorber present) and that observed when the absorbing species is present, $(\beta_{abs} - \beta_{base})$ in eq 5:

$$\text{absorbance} = L/c \times (\beta_{abs} - \beta_{base}) \quad (5)$$

$$\text{absorbance} = nl\sigma \quad (6)$$

The Beer−Lambert law, eq 6, may then be used to extract the unknown absorption cross section σ for spectroscopic experiments or the species number density n for the kinetics experiments. The two lengths L and l in eqs 5 and 6 are intentionally left distinct, because they are not equal in the experiments described here, as will be discussed later. These two relationships apply when the absorption or scattering is small, which is the case in these experiments.

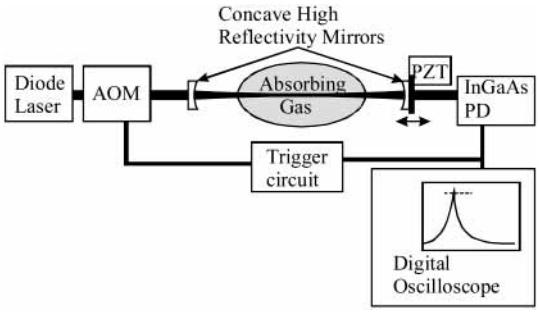

Figure 1. Block diagram of the continuous laser excitation cavity-ring down (CWCRD) near-IR spectrometer described in the text.

In the experiments reported here (see Figure 1), an 86 cm linear cavity is constructed from two 7.5 mm diameter mirrors with a 1 m radius of curvature which have been coated to produce maximum reflectivity at 1310 nm. The mirrors have an observed maximum reflectivity of 99.995%, or a base loss of ca. 50 parts per million per pass (ppmpp) through the cavity, resulting in ring down times (the inverse of β) of the order of tens of μs.

The excitation laser is an InGaAs external cavity tunable diode laser (New Focus, Inc., model 6248) or ECDL, which produces up to 5 mW of approximately 1 MHz bandwidth light, tunable from about 1275 to 1348 nm with few mode hops. There are two scanning modes which may be used in spectroscopic experiments: a coarse mode with a wavelength step of 0.01 nm tunable across the whole range of the laser and a fine mode with a wavelength step of approximately 60 MHz over a range of about 60 GHz (or about 0.29 nm at 1310 nm.) The absolute frequency stability of the ECDL is sufficient to produce a stationary wavelength position (with respect to the breadth of the spectral features) over the course of hours for the kinetics measurements. The fact that the laser bandwidth is narrow compared to the absorption feature is favorable for quantitative concentration determination by absorption experiments in general and especially for cavity ring-down.[122]

The first-order diffracted beam from an InP acousto-optic modulator (AOM) is delivered to the cavity through a mode-matching lens. Using a Faraday rotator opto-isolator was observed to result in weaker light injections into the cavity, so it was removed. The light exiting the cavity is detected by an amplified InGaAs photodiode (New Focus 8130) with a signal bandwidth of 50 MHz. A trigger circuit is used to detect the presence of a preset light-induced signal level and to start the ring-down measurement by interrupting the light to the cavity using the AOM and by triggering the oscilloscope. The ring-down signals are digitized by a 400 MHz 1 GSample/sec 8-bit digital oscilloscope (Tektronix TDS-3052). Individual ring-down signals are transferred to a Pentium computer via the IEEE-488 interface, and the decay constants are determined by a nonlinear Levenberg−Marquardt fit (Labview VI, National Instruments, Inc). Ring-down signals are not averaged in the oscilloscope because the photolysis laser produces different concentrations of radicals on each shot, and the sum of exponential decays with different time constants (corresponding to different absorbances and hence photon loss rates) is *not* an exponential. This is an important factor in ring-down experiments that seek to measure transient species. The spectroscopic or kinetic data are logged for further display or analysis.

To induce light build-up in the cavity, the "pseudolocking" strategy is used because it is less experimentally demanding.[82,83] The length of the cavity is modulated at frequencies between 1 and 20 Hz over a distance greater than the full free spectral

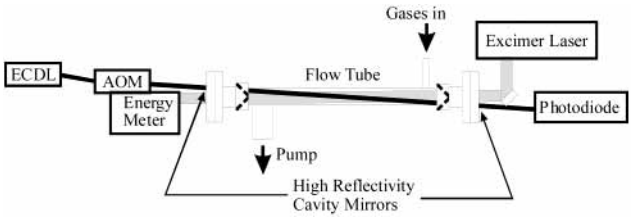

Figure 2. Diagram of the pulsed photolysis-CWCRD kinetic reactor system. The overlap of the excimer photolysis laser and the near-IR probe laser is approximately to scale, but the probe beam appears nearer to the walls of the flow reactor than it is in reality.

range, resulting in a reliable introduction of light into the ring-down cavity at least once per cycle. The cavity length is modulated by a piezoelectric element on the drive screw of a linear translation mount to which the cavity mirror mount nearest the detector is attached. The piezoelectric is driven by a triangular ramp voltage waveform produced by a computer controlled function generator (PCI-330, PC Instruments, Inc.)

The Slow-Flow Reactor. The cavity ring-down mirrors are cemented to the inside of deep-UV grade quartz windows which then are attached to the flow reactor system, illustrated in Figure 2, by standard vacuum (ConFlat) flanges. Only gas phase species come between the reflective surfaces of the mirrors, as required for low-base-loss ring-down experiments. The near-infrared laser beam may be slightly attenuated by scattering or absorption as it goes through the quartz flats, but these losses are external to the cavity and are thus considered unimportant in the ring-down experiment, as long as they are fairly small. The flanges containing the optics attach to molded bellows which mate to 1.5 in. tubing compression fittings. These hold the central region of the flow reactor in which the radical reactions take place, a 1.5 in. OD glass tube approximately 50 cm in length with half inch tubing inlets for pumping and introduction of the gas flow and 0.25 in. inlets for pressure measurement. The ends of the vacuum flange system are held in large true gimbal mounts, which allow for fine alignment of the cavity mirrors. The gimbal mount nearest the detector is held on a linear translation stage which is driven by a piezo-transducer to modulate the cavity length.

The flows of gases and vapors are controlled by calibrated mass flow controllers (MFC, Tylan FC-230) and bubblers which are maintained at constant temperature and pressure. A large excess of an inert buffer, usually nitrogen (a few early experiments used helium), is always present. For the kinetic studies, approximately 20% oxygen gas is added to make peroxy radicals from alkyl radicals. The alkyl radicals are produced by the photolysis of suitable precursors which were delivered from the pure liquids using bubblers. A single-stage rotary pump is used to evacuate the reactor, resulting in a refresh rate of approximately 1 Hz (the inverse of the mean time required for a species to move from the inlet to the outlet of the reactor.) The pressure in the reactor is measured with a combination pressure gauge (Hastings-Teledyne HPM-2002) and can be adjusted by regulating the inlet flow rate and/or the outlet pumping rate (using a needle valve). Commercial grade helium (99.9%), nitrogen (99.9%), oxygen (99.6%), nitric oxide (99%), and ethane (99%) gases and HPLC grade 3-pentanone (96.0%), reagent grade ethyl bromide (98%) and carbon tetrachloride (99.8%), and practical grade acetaldehyde (99%) were all used as supplied. All experiments were conducted at room temperature, 297 K.

A small flow (50−100 standard cm^3 per minute, =10% of the reaction mixture flow) of clean, dry nitrogen is admitted immediately in front of each of the cavity mirrors and goes inward through the vacuum fittings and bellows, finally joining the main flow. This back-flush flow is used to keep the mirrors from becoming contaminated by the precursors, reagents, and radicals in the main flow. We have observed that this simple strategy allows the mirrors to remain clean enough to use for weeks at a time.[110] The regions where the back-flush flow joins the main flow also act as barriers, defining the region where the radical chemistry is expected to take place. Clearly, this does not lead to sharp boundaries for the flow, but our past experience is that the path length calculated from the observed absorbance of species with known absorption cross-section and concentrations is consistent with the length of the central flow zone.[110]

Excimer Laser Photolysis. The geometry of the slow-flow reactor and photolysis beam is shown in Figure 2. The concept is similar to that reported by Yu and co-workers[85] except that the use of small (7.5 mm diameter) ring-down cavity mirrors allows the photolysis and ring-down laser beams to be much closer, providing significant overlap of the photolysis and probe (CWCRD) beams with a shorter overall cavity length (86 cm). The flow reactor is divided by the entrance and pumping ports into three zones: the central zone (36 cm) between the main entrance and pumping ports contains the complete mixture of reactant(s), photolytic precursor, and buffer gas, whereas the zones near the mirrors are filled with the nitrogen back-flush flow. The photolysis laser (Questek 2560 Excimer, ArF, 193 nm, <50 mJ/pulse, ~20 ns pulse width) is slightly larger than 1 in. wide and is directly adjacent to the 7.5 mm mirrors at each end of the cavity. This results in a crossing angle of about 1.1° and complete inclusion of the cavity ring-down probe beam within the photolysis beam path inside of the central 36 cm of the reactor, establishing this distance as the path length for the absorbance measurement immediately following the initiation of the chemistry.

Four photolytic precursor molecules were used in the current experiments: 3-pentanone and ethyl bromide for ethyl radicals, acetone for methyl radicals, and carbon tetrachloride for chlorine atoms. The ketones are the cleanest systems, producing essentially only the alkyl radicals (two per molecule) and carbon monoxide,[2] which was inert in our reaction system. Once the alkyl radicals were formed, they reacted (via Reaction 1) within microseconds with the oxygen in the flow to produce the desired alkyl peroxy radicals:

$$CH_3COCH_3 + h\nu \rightarrow 2CH_3 + CO\ (\sim 100\%) \qquad (7)$$

$$CH_3CH_2COCH_2CH_3 + h\nu \rightarrow 2CH_3CH_2 + CO\ (\sim 100\%) \qquad (8)$$

Ethyl bromide produced ethyl radicals and bromine atoms. Finally, 193 nm photolysis of carbon tetrachloride breaks either one or two carbon−chlorine bonds with nearly equal probability,[10] resulting in chlorine atoms and both CCl_3 and CCl_2:

$$CCl_4 + h\nu \rightarrow CCl_3 + Cl\ (46\%) \qquad (9)$$

$$CCl_4 + h\nu \rightarrow CCl_2 + 2Cl\ (53\%) \qquad (10)$$

The chlorine atoms were allowed to react with ethane to yield ethyl radicals or with acetaldehyde to give acetyl radicals which rapidly reacted in our system to eventually produce methyl radicals. (In reaction 12, acetyl radicals react with oxygen to produce acetyl peroxy radicals which rapidly self-react to form

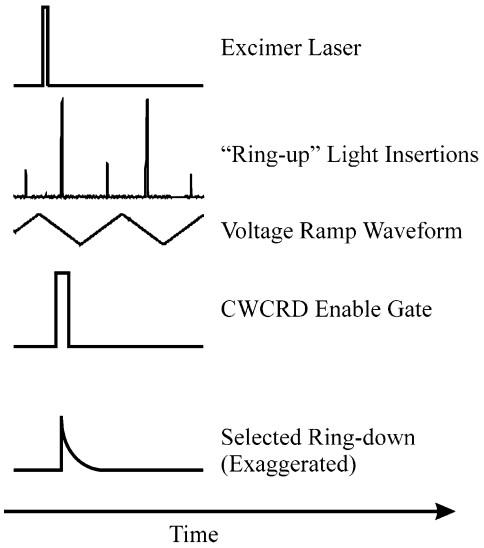

Figure 3. Timing diagram for the pulsed photolysis CWCRD setup which allows transient spectroscopy with the pseudolocking scheme. The widths of the excimer laser and the ring-down event are greatly exaggerated for clarity.

the CH_3CO_2 radical which spontaneously decomposes giving CH_3 and carbon dioxide, all within less than 1 ms.)

$$Cl + C_2H_6 \rightarrow HCl + C_2H_5 \quad (11)$$

$$Cl + CH_3CHO \rightarrow CH_3CO \rightarrow CH_3C(O)O_2 \rightarrow CH_3C(O)O \rightarrow CH_3 + \text{other products} \quad (12)$$

Ethyl bromide photolysis coproduces a bromine atom, whereas CCl_4 photolysis yields both the CCl_3 and CCl_2 radicals, all of which could be reactive in our system, so these precursor systems were only used for the proof of spectral carrier experiments and not in the kinetic experiments.

Timing Strategies. To conduct pulsed photolysis experiments on either the kinetics or the spectroscopy of radicals, the timing between the photolysis and cavity ring-down events must be controlled. No direct control over the timing of the cavity ring-down event is provided in the pseudolocking approach used to allow photons to get into the cavity in these experiments. Solutions to this problem were explored for the spectroscopic and kinetics experiments, and the most useful are described here. A timing diagram for the experiment is presented in Figure 3, with some of the time widths exaggerated to make the events visible. The introduction of light into the cavity by the periodic modulation of the cavity length was found to result in a quasistable timing relationship between the ring-down signal and the ramp waveform, with a long-term stability of minutes and a delay time jitter of ~1 ms. This relationship was used to establish approximate control over the delay time between the ring-down event and the excimer laser (which was synchronized to the cavity length modulation waveform). The frequency of the modulation waveform (usually 10−20 Hz) needs to be much larger than the repetition rate of the photolysis laser (which must be 2 Hz or less to guarantee that a fresh reaction mixture is present for each laser shot) in order to achieve stable introduction of light into the ring-down cavity. The ramp waveform, produced by a PC mounted analog function generator (PC Instruments, PCI-330), was an asymmetric triangle wave with software-controllable duty cycle, frequency, and amplitude (typical values: 80% positive duty cycle, 10 Hz, 1.5 Vp-p). The ramp waveform is sent to a piezo-electric controller and actuator (ThorLabs MDT694/PE4) that drives a linear translation stage holding the end of the cavity. The function generator also provides a square wave synch output which was used to control the firing of the photolysis laser, after a 5 or 10 times frequency division. The delay time between the photolysis pulse and the start of a cavity length modulation cycle is controlled by a digital delay circuit, allowing the delay to the ring-down signal to be smoothly varied over one period of the ramp waveform. Alternatively, the time between the excimer laser and the ring-down event can be coarsely controlled by varying the DC offset of the voltage ramp, which causes the ring-down signal to change position with respect to the ramp waveform. The former approach produces much more reliable ring-down signals and timing.

The above strategy "controls" the delay between photolysis and probe events within the window of the modulation period (50−100 ms) with an uncertainty of ~2 ms. (Because the modulation is periodic and at least one ring-down event occurs per cycle, the modulation period is the maximum delay necessary with this strategy.) For the spectroscopic studies, it is desirable to measure the concentrations of the radicals as soon as possible after their formation. For the kinetics, the delays are randomly varied over the total reaction time to minimize long-term drift effects. To ensure that only ring-down signals with the proper timing relationship to the photolysis pulse are used for the spectroscopic (and the kinetics) experiments, an enable gate is used to select the light introductions which triggered ring-down data workups. All potential ring-downs outside of the gate are ignored. The width and delay of the enable gate with respect to the photolysis laser pulse are controlled by a digital delay generator. Typically, the gate is 3 ms long to enhance the probability of capturing the jittering ring-down signal and is set at approximately 0.5 ms for the spectroscopic experiments (essentially at zero reaction time for the peroxy radical's slow self-reaction) or at variable reaction times for the kinetic experiments. This gate width is appropriate for the slow reactions studied here but can easily be narrowed for the study of faster reactions. The limitation for fast kinetic studies in this mode is the assumption that the concentration of the transient species is constant over the ~100 μs ring-down decay, but it is also possible to monitor kinetics which are faster than the ring-down.[111]

The majority of the spectroscopic and kinetic results for the peroxy radicals presented here were obtained using the gating strategy. The drawback is that it is inefficient, both in terms of total data throughput and wasted photolysis shots. An alternative solution was explored which provides a definitive timing relationship between the photolysis pulse and cavity ring-down probe. In this approach, the natural delay time variation of the ring-down event allows for semirandom sampling of time, and this is coupled with a measurement of the delay (and hence reaction) time for the kinetics studies. In this case, the width of the enable gate is set for the total reaction time (usually a few hundred ms), and the time difference between the photolysis pulse and the cavity ring-down signal is measured using a PC mounted digital counter/timer (Measurement Computing, CIO-DIO-9054 CTR). The enable gate is used in this method because increasing the delay between the excimer pulse and the beginning of the gate allows sampling of the later reaction times (the first ring-down to occur in the gate is the one that is recorded.) This method resulted in a more satisfactory data collection rate of one ring-down per photolysis shot. In principle, it would be possible to accumulate more than one ring-down per excimer laser pulse, but this would require more than one

active counter/timer channel and some way of controlling the sequence of the channels. In this approach, the reaction time could also be established with greater precision (1 μs) than in the gated experiment. The major drawback of this method is greater scatter in the kinetic data. In the gated strategy, multiple ring-down-determined absorbance measurements can be averaged at the same reaction time (to within the width of the gate) to produce higher signal-to-noise, which cannot be done easily with the random time sampling. We are investigating binning and/or smoothing strategies that can be used to filter some of the noise from the kinetic results before they are subjected to the modeling/fitting procedure described below.

Experimental Overview. In both the spectroscopic and kinetic experiments, the time to complete the ring-down measurement is less than 200 μs, essentially instantaneous on the time scale of the peroxy radical decay. This separation of time scales means that the concentration of radicals, and hence the absorbance, is constant during the ring-down. The absorbance (or the related concentration) can then be studied at a fixed reaction time as a function of wavelength, or at a fixed wavelength as a function of reaction time, as is true of most transient absorption measurements. In the spectroscopy experiments, the timing between photolysis and cavity ring-down events was fixed, using the enable gate, and the wavelength of the laser was scanned stepwise while multiple CWCRD absorbance measurements were averaged at each wavelength position. The cavity length is modulated on a fast time scale, whereas the ECDL laser is stepped on a much slower time scale as the absorbance data are accumulated. At each wavelength position, the timing and the DC level of the cavity-length modulation ramp waveform were adjusted to bring the ring-down signals within the enable gate. This is necessary because changing the CWCRD laser wavelength changes the cavity length resonance condition ($L \approx n\lambda/2$), which is reflected as a change in the position of the ring-down signal with respect to the ramp. In the gated kinetics experiments, the ECDL wavelength is fixed and the delay time for the enable gate is entered on the digital delay generator, setting the reaction time for a single kinetic point. Then the time delay between the ramp and the excimer laser is used to bring the ring-down signal into the gate. (Because the laser wavelength is constant in the kinetics experiment, the ring-down signal is usually more stable than in the spectroscopy experiment.) After averaging the desired number of ring-down-determined absorbance measurements, the entire procedure is repeated at a different reaction time until the radical decay curve is constructed. In the random sampling/time measurement kinetics strategy, the user only has to change the gate delay occasionally to ascertain that the total reaction time window is adequately sampled, as described above.

Kinetic Data Processing. For simplicity and to be consistent with the earlier report of alkyl peroxy radical absorption cross sections in the near-IR,[2] a simplified treatment was used to extract the EtO_2 and MeO_2 peak absorption cross sections from the measured self-reaction kinetics. The inverse of the absorbance is plotted as a function of time, and the published values of the observed second-order rate coefficients are used to extract the unknown absorption cross-sections. This procedure implies that the secondary chemistry in the self-reaction mechanism (see the Introduction) is rapid and simply amplifies the observed rate of peroxy radical decay, while retaining the shape predicted for the simple bimolecular reaction. These cross sections could then be used in the cross-reaction kinetics.

The peroxy radical cross-reaction kinetic experiments were analyzed using a new version of the ACUFIT computer program, a nonlinear iterative fitting program that was developed for analyzing complex chemical systems. This approach is needed because the observed decay signature of the radical's absorbance is due to a number of reactions, as explained above. The ACUFIT computer program was originally developed by Braun and co-workers at NIST (Gaithersburg, MD) and was recently ported to the Labview platform with some changes to the nonlinear fitting core and considerable improvements to the input/output structure to enhance usability. The ACUFIT program uses the published ACUCHEM[123] program as a core to accomplish the numerical integration of the kinetic mechanism, providing a simulation of the absorbance vs time profile. (The absorption cross sections of all species in the mechanism at the monitor wavelength must be provided.) This simulation is compared to the kinetic data, and selected rate coefficients and initial concentrations of species in the mechanism are varied to obtain the best fit using the Labview Levenberg−Marquardt routine.

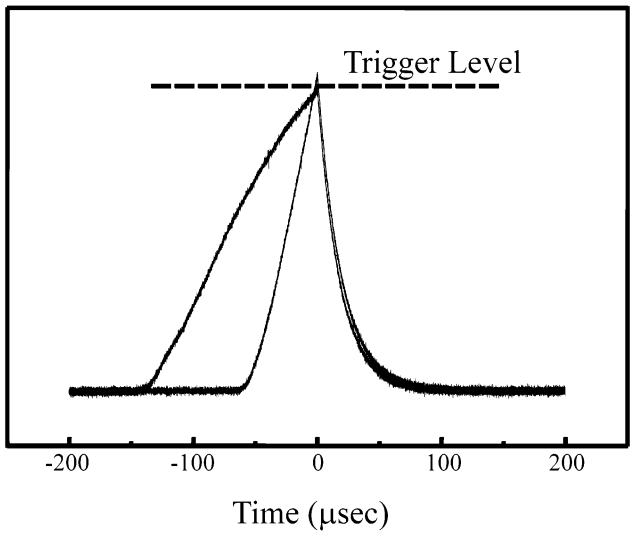

Figure 4. Examples of individual ring-down signals observed in the CWCRD instrument. The two different traces (which are overlaid) are due to "ring-ups" generated at two different laser powers. The two ring-downs are indistinguishable.

3. Results and Discussion

Characterization of the CWCRD Spectrometer. The results of the pseudolocking cavity length modulation procedure are shown in Figure 3, where the voltage ramp waveform and the "ring-up" light insertion events are actual experimental data. The sharp spikes are the light introduction events where the cavity length comes into resonance with the laser. The trigger circuit is disabled, so the reproducibility of the height of the spikes is an indication of the stability of the system. Rapidly modulating the cavity makes the effects of thermal length changes and vibrations inconsequential on the time scale of the experiment. The results obtained with a 10 Hz symmetrical triangle waveform are shown. Clearly, the positive cycle (where the cavity mirror is pushed against the vacuum and spring of the linear translation mount) produces better light injections. We attribute this to backlash in the modulation drive mechanism. Because the positive cycle produces better results, we use an asymmetric waveform with 80% up and 20% down cycles. The trigger level, where the laser is interrupted by the AOM and the ring-down is recorded, is typically set to 50% to 75% of the height of the nontriggered signals.

Sample ring-down traces are shown in Figure 4. Two traces are shown (superimposed) which were recorded at different

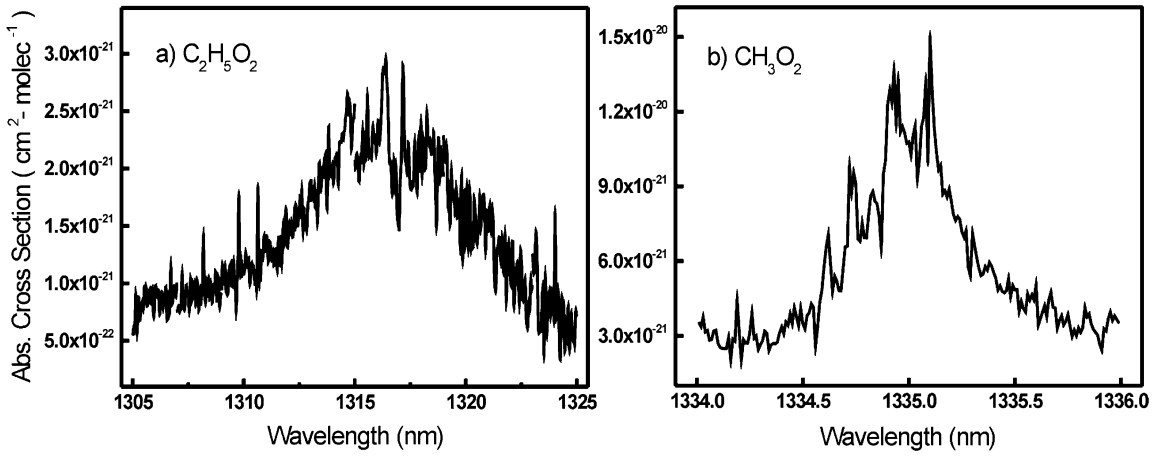

Figure 5. Near-IR transient absorption spectra for EtO_2 and MeO_2, recorded using the pulsed photolysis CWCRD reactor system. Some of the sharp features (both upward and downward) are missing from the spectra of Pushkarsky et al. and are thus probably spurious noise.

excitation laser powers but otherwise identical base conditions (same wavelength and no absorber in the reactor). The signals before the trigger are different because the rate of introduction of photons into the cavity (the ring-up) depends on the incident power. The ring-down signals after the trigger are identical because they only reflect the loss of light intensity from the passive cavity by all light loss mechanisms present, exactly as is done in the pulsed CRD experiment. The high signal-to-noise ratio (>100 near the beginning of the decay) of the ring-down signals is evident. The high S/N ratio results in high precision in the determination of the decay constant β, which shows relative standard deviations of less than 1%, similar to what is observed in pulsed ring-down experiments.[110] With mirror losses of less than 100 ppm (typically 50−70, as determined by the empty cavity ring-downs), this gives a single shot absorbance detection limit of less than 1×10^{-6}. The decay constants are also randomly distributed about a mean and thus averaging can yield further improvement, as is usually observed in ring-down experiments.[86,110,114,124,125]

More careful examination of the ring-up portion of the traces, and comparison to the ring-down, reveals that the rate constant for the introduction of photons into the cavity is the same as that for photons leaving the cavity. The difference in shape between the two traces reflects the different saturation levels which are being approached; the steeper trace is heading for a higher ultimate transmitted intensity because of the higher input power. The fact that the same physical process which is being used to measure species absorptions is responsible for the introduction of light into the cavity has an unfortunate side effect. As the level of absorption or scattering by analytes in the reactor increases, the saturation level (the highest intensity observed during "good" matching of the cavity length to the laser) decreases. The rate of approach to the new lower saturation level also increases, but this is not usually a problem. The decrease of saturation level with increasing absorption or scattering by analytes can bring the peak light intensity value below the preset trigger level, making it impossible to observe ring-downs. This effect can be countered to some extent by dropping the trigger level or by increasing the input laser power. Lowering the trigger level results in a lower S/N ratio on the ring-down signal, because the shot noise and electrical noise remain essentially constant. Increasing the input laser power can be effective, but depending on the feedback levels to the diode laser, coherence collapse is always observed at some finite power.[84] Fortunately, coherence collapse is obvious in this experiment, because the simple single mode cavity length structure shown in Figure 3 collapses into a large number of far less intense signals, reflecting the multimode output of the laser. Presumably better control of optical feedback would help to counter this effect, but in practical terms, the problems of decreasing throughput at higher optical extinction and feedback-induced coherence collapse result in a limit on the upper end of the dynamic range for this measurement. We note that this is not a problem which is encountered in the pulsed CRD experiments.

The NIR Spectra of the Ethyl Peroxy and Methyl Peroxy Radicals. The near-IR transient absorption spectra for EtO_2 and MeO_2 obtained in the pulsed photolysis/CWCRD reactor system are shown in Figure 5. The EtO_2 radicals are produced by 193 nm photolysis of a mixture containing approximately 0.4 Torr of 3-pentanone, 4 Torr of O_2, and balance nitrogen buffer to yield a total pressure of 20 Torr. For MeO_2, the 3-pentanone is replaced by ~0.3 Torr of acetone. The spectra were recorded with a 0.01 nm step size, accumulating and averaging five ring-down decay measurements per wavelength step. High resolution scans with a smaller step size (using the fine scan mode of the ECDL) did not display any additional spectral structure and thus are not shown. These spectra were obtained with a fixed enable gate width (see the Experimental Section for a description of this parameter) of 3 ms and delay time of 0.4 ms. The kinetic traces presented below indicate that this represents the peak value of the absorbance, which is essentially constant over the gate width. The shape and position of these spectra are consistent with the two earlier reports of the MeO_2 and EtO_2 near-IR spectra, one of which used pulsed CRD and the same photolysis conditions.[1,2] In the case of the EtO_2 spectrum, the photolysis laser power changed continuously during the run (which took about 10 h), and thus, a linear power correction was applied. The absorption cross sections (base e) are thus best defined at the peaks near 1316.4 and 1317 nm as determined by the kinetics measurements described below, and those at other wavelengths are more uncertain.

The identity of the spectral carriers was also supported by recording the spectra using alternate photolytic precursors, by confirming that the absorption signals were transient in nature and by investigating the absorbance's dependence on photolysis intensity and radical precursor and molecular oxygen number density. Three photolytic precursors for EtO_2 were used, including the 3-pentanone. Ethyl bromide, C_2H_5Br (0.3 Torr), was photolyzed at 193 nm, producing an ethyl radical and a bromine atom. The ethyl radical reacts with oxygen, and the resulting absorbance decay (of $C_2H_5O_2$) is similar to that

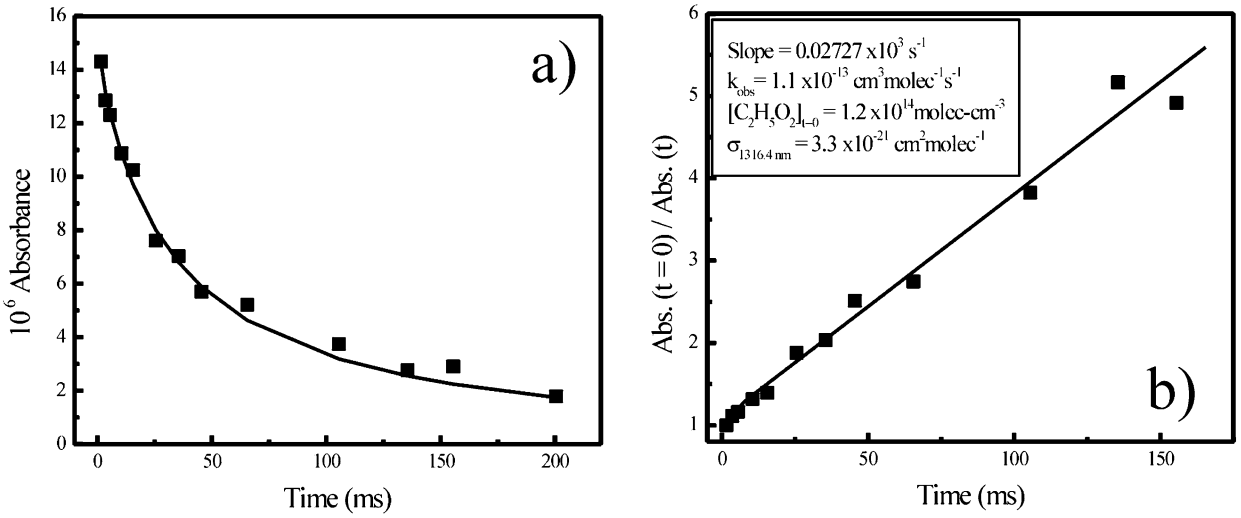

Figure 6. Self-reaction kinetics of EtO_2 observed via near-IR absorbance at 1316.4 nm. The linear form on the right was used to obtain the absorption cross section for the radical.

produced in the photolysis of pentanone. The fate of the bromine atom in this system is unclear. The spectrum of EtO_2 between 1315 and 1318 nm produced by ethyl bromide is similar to that produced using the photolysis of 3-pentanone, but it was increasingly difficult to obtain CWCRD spectra beyond this wavelength range because of the absorption by the parent ethyl bromide. Spectral interference problems from precursors and other stable components in the reaction mixture encountered in pulsed CRD spectroscopy[126] are compounded in CWCRD, where the "ring-up" of photons is impeded by absorbers, both transient and stable. Photolysis of carbon tetrachloride was used to produce chlorine atoms, which could then be used to abstract a hydrogen atom from ethane. Subsequent reaction of the ethyl radical with O_2 created EtO_2, whereas reaction of the CCl_3 and CCl_2 radicals (coproduced in the photolysis) with oxygen presumably resulted in the formation of reactive CCl_3O_2 and CCl_2O_2 peroxy radicals. This presumption is supported by the fact that the transient absorbance decayed more rapidly than in either of the other two photolysis systems. The spectrum obtained from this third system again shows the same features as that of the 3-pentanone photolysis. In the two alternate photolysis systems (ethyl bromide and CCl_4/ethane), there was no clear indication of absorption by the other peroxy radicals. The similarity of the three transient absorption spectra near 1317 nm supports the assignment of spectral carrier as EtO_2. The confirmation of spectral carrier for the MeO_2 system was already reported by Pushkarsky et al. using alternate photolysis precursors.[2]

For additional confirmation of spectral carriers and for the kinetic work below, measurements were conducted at fixed wavelengths corresponding to observed maxima in the spectra. For EtO_2, this was either 1317.01 or 1316.40 nm, where the latter was found to be preferable because it is broader and hence less susceptible to laser drift. For MeO_2, the single strong peak at 1335.07 was used. The transient nature of the absorbance is illustrated below in the kinetic results section. The peroxy radicals are formed immediately after the photolysis pulse and exhibit second order decays with first half-lives of tens of milliseconds, slightly faster for MeO_2 than for EtO_2. The absorptions are only present when the photolysis laser is present (a given, because the mixture in the absence of photolysis is the base condition in the extraction of absorbance by eq 5.) The absorbance is linearly dependent on photolysis power. The production of a transient absorbance is also found to depend on the presence of oxygen, although our experiments indicate that much less O_2 could be used with little loss in radical production, as expected for the large pseudo-first-order rate predicted for the ethyl-radical−oxygen addition reaction.[127] For methyl radicals, more oxygen may be needed because of the lower oxygen addition rate. The near-IR absorbance for each radical is also found to depend linearly on the precursor concentration, until the assumption of small absorbance in the photolysis is violated. The assumption of optically thin media in the photolysis is never particularly valid because in order to produce measurable amounts of radicals we have to use precursor concentrations that give about 10% absorbance of the photolysis beam. Efforts are currently under way to deliver more of the ~50 mJ/pulse which our excimer laser produces to the system so that the precursor concentration could be decreased, while still producing adequate initial concentrations to follow the signal for greater than three half-lives in the kinetic measurements.

The experiments described above all demonstrate that the observed absorption signatures depend as expected on the details of the formation system and are thus most likely due to EtO_2 and MeO_2. The absorbance at the two monitor wavelengths, 1316.4 nm for EtO_2 and 1335.1 nm for MeO_2, could thus be used to measure the concentrations of the two radicals with minimal spectral crossover, once the previously unknown absorption cross sections for the two radicals were measured.

Absorption Cross Section Determinations. The absorption cross sections of EtO_2 were measured at the peak of the sharp band near 1317 nm and on the broader band at 1316.4 nm by observing the self-reaction kinetics of the radical. The recommendation[4,7] for the observed self-reaction rate coefficient k_{obs} (which includes the influence of secondary chemistry) is used in the fitting of the data to determine the unknown absorption cross section. This method was used previously to establish the cross section of the MeO_2 origin band near 1357 nm.[2] One set of data used in this procedure is shown in Figure 6, both in the normal decay format of absorbance vs time and in the linear form which was used in the extraction of the absorption cross section.

The linear form is produced by rearranging the integrated rate expression, eq 13, to the form in eq 14, which involves a ratio of measured absorbances:

$$[C_2H_5O_2]^{-1} = [C_2H_5O_2]_{t=0}{}^{-1} + 2k_{obs}t \quad (13)$$

$$Abs(C_2H_5O_2,t=0)/Abs(C_2H_5O_2,t) = 1 + 2k_{obs}t[C_2H_5O_2]_{t=0} \quad (14)$$

The slope of the best fit line in Figure 6b thus allows extraction of the initial concentration of EtO_2, using the recommended value of $k_{obs} = 1.1 \times 10^{-13}$ cm^3 molecule^{-1} s^{-1}.[7] This initial concentration, combined with the known path length, 36 cm, and the measured initial absorbance yields a value for the cross section of $\sigma_{1316.4}(C_2H_5O_2) = 3.0\ (\pm 1.5) \times 10^{-21}$ cm^2 molecule^{-1}, where Beer−Lambert behavior (eq 6) is expected to be observed for these small total absorbances. Interestingly, the cross section at the sharp peak near 1317 nm is observed to be identical to that at 1316.4 to within the precision of the measurements. The precision of these measurements (five replicates at 1316.4 nm and two at 1317 nm) is within 10%, but the uncertainty in the recommended observed rate coefficient of ~30% has to be factored into the total uncertainty in the absorption cross section quoted above, so we assign the fairly generous error limits of 50%.

The procedure above was then repeated for MeO_2 at the sharp peak near 1335 nm. One set of results are shown in Figure 7. The recommended[4,7] value of $k_{obs} = 4.9\ (\pm 0.5) \times 10^{-13}$ cm^3 molecule^{-1} s^{-1} allowed us to derive the absorption cross section $\sigma_{1335.1}(CH_3O_2) = 1.5\ (\pm\ 0.8) \times 10^{-20}$ cm^2 molecule^{-1}. A good test of this system would have been to verify the absorption cross section for the origin band of MeO_2 reported by Pushkasky, but that band is outside of the tuning range of our diode laser.

Both radicals' absorbances were also measured at the other's maximum absorption and were found to contribute less than 10% of the observed composite signal. This was used to estimate a value for the cross-contamination absorption cross-sections for the fitting. We will be able to improve on these estimates in future kinetic work by measuring the photolysis laser power with and without the precursors present.

Ethyl Peroxy−Methyl Peroxy Cross-Reaction Kinetics. To measure the reaction kinetics of the cross-reaction between the two different peroxy radicals, the same procedure was followed as for the self-reaction, except that both radical precursors, acetone and 3-pentanone, were present. Then, optimally, measurement of the absorbance decay would be recorded at both monitor wavelengths, 1316.4 nm for $C_2H_5O_2$ and 1335.1 nm for CH_3O_2, with as close to the same conditions of flow and photolysis as possible. In the experiment shown in Figure 8, the concentration of the acetone was too high when the EtO_2 experiment was conducted. This is reflected in the fact that the initial absorbance in the 1316.4 nm data is quite different between the self-reaction run (squares) and the cross-reaction run (circles) because the acetone interfered with the 3-pentanone's absorption of the photolysis beam (both photolysis absorptions were ~25%). It became apparent that the concentrations of the two precursors needed to be adjusted to produce ~10% (or less) absorbance of the excimer laser beam. A fast laser energy meter is being procured to allow the measurement of the excimer absorbance, which will also allow for better verification of the initial concentrations of the radicals. Despite these less than ideal experimental conditions, the data at 1316.4 nm are well-fitted using the ACUFIT program with our experimentally determined values of the absorption cross sections and published values for the reaction rate coefficients and branching ratios.[4,6,7,10] These fits are the solid lines in Figure 8.

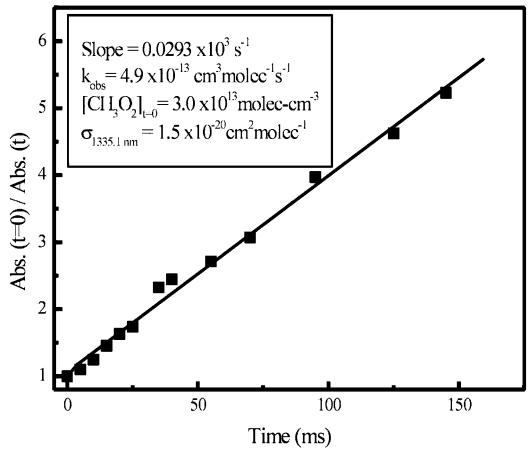

Figure 7. Self-reaction kinetics of MeO_2 used to determine the near-IR absorption cross section.

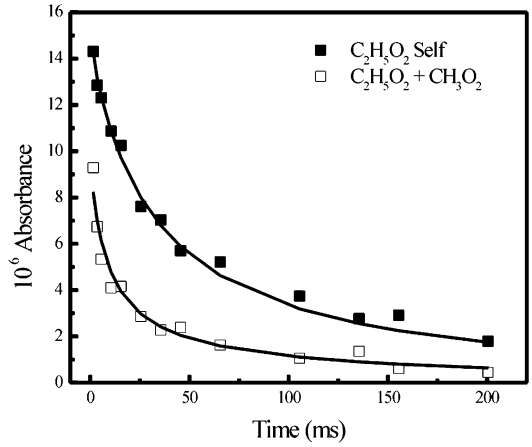

Figure 8. Self-reaction and cross-reaction kinetic measurements for EtO_2 observed at 1316.4 nm. The filled squares are when only the 3-pentanone precursor is photolyzed and the empty squares are when acetone is added to the flow. The lines are obtained from the modeling/fitting routine described below.

The mechanism used is given in Table 1 below, and the only parameter which was allowed to vary in the fit was the cross-reaction rate coefficient, which was found to be $k(CH_3O_2 + C_2H_5O_2) = 2.0\ (\pm 1.0) \times 10^{-13}$ cm^3 molecule^{-1} s^{-1} at 297 K and 20 Torr.

The results of the simulation generated by ACUFIT using the mechanism in Table 1 are shown in Figure 9. The concentration vs time profiles generated by the integration of the mechanism are then multiplied by the absorption cross sections (and path length) of all potential absorbers at the monitor wavelength and the compound absorbance is compared to the kinetic data. The concentration of MeO_2 is observed to decrease more rapidly than that of EtO_2, as expected. The concentrations of HO_2 and the alkoxy radicals CH_3O and C_2H_5O are found to be significantly lower than those of the peroxy radicals. This is unfortunate, because following these species during the course of the reaction would further constrain the fit and produce much less uncertainty in the derived rate coefficients. The hydroperoxy radical also has a near-IR absorption, but it is of comparable absorption cross section to the alkyl peroxy radicals, so it would be nearly impossible to monitor with this method.

The generous error bars on the cross-reaction rate coefficient reflect an attempt to be conservative on our part. The assignment of the uncertainty in complex fits of this type requires a good knowledge of the uncertainty of each of the individual param-

TABLE 1: Reaction Mechanism Used to Model the Cross-Reaction of $CH_3O_2 + C_2H_5O_2$ and Obtain Fits (Figure 9) to the Kinetic Data[a]

reaction	k(298 K) cm^3 molecule^{-1} s^{-1}	branching ratio	ref
$CH_3O_2 + CH_3O_2 \rightarrow 2\ CH_3O + O_2$	4.7×10^{-13}	0.33	127
$\rightarrow CH_3OH + HCHO + O_2$		0.67	
$C_2H_5O_2 + C_2H_5O_2 \rightarrow 2\ C_2H_5O + O_2$	6.8×10^{-14}	0.63	127
$\rightarrow C_2H_5OH + CH_3CHO + O_2$		0.37	
$CH_3O_2 + C_2H_5O_2 \rightarrow CH_3O + C_2H_5O + O_2$	2.0×10^{-13}	0.49	3, this work
$\rightarrow CH_3OH + CH_3CHO + O_2$		*b*	
$\rightarrow C_2H_5OH + HCHO + O_2$		*b*	
$CH_3O + O_2 \rightarrow HCHO + HO_2$	1.9×10^{-15}	1	127
$C_2H_5O + O_2 \rightarrow CH_3CHO + HO_2$	1.0×10^{-14}	1	127
$CH_3O_2 + HO_2 \rightarrow CH_3OOH + O_2$	5.6×10^{-12}	~1	127
$C_2H_5O_2 + HO_2 \rightarrow C_2H_5OOH + O_2$	8.0×10^{-12}	~1	127

[a] The branching ratios are the rate coefficient for the channel divided by the sum of the rate coefficients for all channels for that reaction. [b] The branching ratio of the cross-reaction into the radical propagating channel has been estimated by the arithmetic mean of the two self-reaction branching ratios, and no data exists on these ratios to the best of our knowledge.

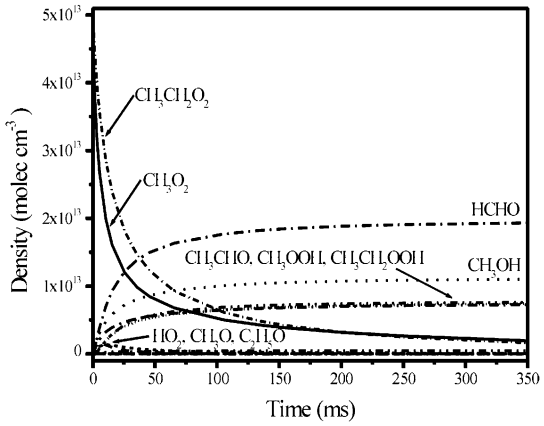

Figure 9. One simulation run of the modeling program, ACUCHEM. The absorption cross sections and path length would then be used in ACUFIT to compare the simulation with the kinetic data, and the rate coefficients or initial concentrations could be adjusted to obtain the best fit.

eters in the mechanism and a careful systematic examination of the effects of each of these uncertainties on the rate coefficient which is being derived.[3,58] We have not completed this careful assessment of uncertainty to date and would prefer to obtain more kinetic data to get a better idea of the precision in the fits before we do so.

4. Conclusions

The CWCRD system was shown to possess good resolution and sensitivity, comparable with many state-of-the-art ring-down and other sensitive absorption-based spectroscopic methods. By incorporating the CWCRD spectrometer into a more traditional pulsed laser photolysis/slow flow reactor system, we are now able to measure the near-IR absorption spectra and reaction kinetics of radicals. The structured electronic transitions of peroxy radicals can be used to follow the concentrations of individual peroxy radicals in kinetic studies. In general, the spectra and absorption cross sections of the peroxy radicals need to be measured first, but we have demonstrated that this is possible, using the prototypical EtO_2 and MeO_2 radicals. The CWCRD spectrometer is also capable of sensitively measuring low concentrations of water vapor and other atmospherically relevant compounds on sharp lines where other absorptions would be unlikely to be present. This may have some important applications in in situ atmospheric monitoring.

The experiments on the EtO_2-MeO_2 cross-reaction were meant primarily to provide a proof of principle for the kinetic methods, but data obtained in the current study are also of use in atmospheric chemistry. First, the absorption cross sections obtained in this work are in (at least) qualitative agreement with those obtained in the earlier study of MeO_2, assuming that similar amounts of MeO_2 were present throughout their reported spectra.[2] Because these absorption cross sections are well below the lowest values used as surrogates in the recent modeling study, $\sigma_{max} = 8 \times 10^{-20}$ cm^2 $molecule^{-1}$, it would appear that the potential role of peroxy radical near-IR photolysis reactions in production of atmospheric OH radicals is not supported.[17] It would still be interesting, and potentially important in the interpretation of the laboratory kinetics, to study the photochemical reaction of the peroxy radicals with near-IR radiation. The lack of observable rotational structure in the spectra of the peroxy radicals measured by both ring-down experiments,[2] especially for EtO_2, may be due to homogeneous broadening and may imply a dissociative or predissociative character in the upper state (or it could just be due to spectral congestion). Because the hydroxyl radical may be sensitively detected using laser induced fluorescence, whereas the peroxy radical's near-IR absorption can be observed in the CWCRD system, some form of action spectroscopy might be able to determine the extent to which this interesting dissociation channel is active.

The determination of the rate coefficient for the cross-reaction reported in this study must be reproduced before it can be considered a high quality measurement, comparable to those in the previous reports.[3] However, the agreement between our measurement and the previously obtained value is compelling. This method appears to hold promise for the investigation of peroxy radical cross-reaction kinetics at arbitrary temperatures and pressures. We are currently making modifications to the flow reactor to obtain temperature control (pressure may be simply controlled by varying the inert buffer flow and/or throttling the pump, as in most slow flow systems), and we are beginning a systematic study of the cross-reaction as functions of both temperature and pressure. Next, we intend to turn our attention to other peroxy radical systems which have not been as extensively studied as the MeO_2-EtO_2 system.

Acknowledgment. The authors thank the Atmospheric Research Group at Portland State University, especially Drs. Robert O'Brien, Thomas Hard, and Linda George for extensive experimental assistance and many useful discussions. Acknowledgment is made to the donors of the Petroleum Research Fund, administered by the American Chemical Society for support of this research.

References and Notes

(1) Hunziker, H. E.; Wendt, H. R. *J. Chem. Phys.* **1976**, *64*, 3488.
(2) Pushkarsky, M. B.; Zalyubovsky, S. J.; Miller, T. A. *J. Chem. Phys.* **2000**, *112*, 10695.
(3) Villenave, E.; Lesclaux, R. *J. Phys. Chem.* **1996**, *100*, 14372.
(4) Alfassi, Z. B. *Peroxyl Radicals*; Wiley: New York, 1997.
(5) Seinfeld, J. H.; Pandis, S. N. *Atmospheric Chemistry and Physics: From Air Pollution to Climate Change*; John Wiley & Sons: New York, 1998.
(6) Wallington, T. J.; Dagaut, P.; Kurylo, M. J. *Chem. Rev.* **1992**, *92*, 667.
(7) Lightfoot, P. D.; Cox, R. A.; Crowley, J. N.; Destriau, M.; Hayman, G. D.; Jenkin, M. E.; Moortgat, G. K.; Zable, F. *Atmos. Environ.* **1992**, *26A*, 1805.
(8) Tyndall, G. S.; Cox, R. A.; Granier, C.; Lesclaux, R.; Moortgat, G. K.; Pilling, M. J.; Ravishankara, A. R.; Wallington, T. J. *J. Geophys. Res.* **2001**, *106*, 12.
(9) Carter, W. P. L. *Atmos. Environ.* **1990**, *24A*, 481.
(10) Atkinson, R.; Baulch, D. L.; Cox, R. A.; Hampson, R. F., Jr.; Kerr, J. A.; Rossi, M. J.; Troe, J. *J. Phys. Chem. Ref. Data* **1997**, *26*, 521.
(11) Carter, W. P. L. *J. Air Waste Manag. Assoc.* **1994**, *44*, 881.
(12) Cox, R. A. *J. Geophys. Res.* **1999**, *104*, 8047.
(13) Derwent, R. G.; Jenkin, M. E.; Saunders, S. M.; Pilling, M. J. *Atmos. Environ.* **1998**, *32*, 2429.
(14) Kleinman, L.; Lee, Y.-N.; Springston, S. R.; Lee, J. H.; Nunnermacker, L.; Weinstein-Lloyd, J.; Zhou, X.; Newman, L. *J. Geophys. Res.* **1995**, *100*, 7263.
(15) Sillman, S. *Annu. Rev. Energy Environ.* **1993**, *18*, 31.
(16) Stevens, P. S.; Mather, J. H.; Brune, W. H.; Eisele, F.; Tanner, D.; Jefferson, A.; Cantrell, C.; Shetter, R.; Sewall, S.; Fried, A.; Henry, B.; Williams, E.; Baumann, K.; Goldan, P.; Kuster, W. *J. Geophys. Res.* **1997**, *102*, 6379.
(17) Frost, G. J.; Ellison, G. B.; Vaida, V. *J. Phys. Chem. A* **1999**, *103*, 10169.
(18) Madronich, S.; Calvert, J. G. *J. Geophys. Res.* **1990**, *95*, 5697.
(19) Brinck, T.; Lee, H.-N.; Jonsson, M. *J. Phys. Chem. A* **1999**, *103*, 7094.
(20) Blanksby, S. J.; Ramond, T. M.; Davico, G. E.; Nimlos, M. R.; Kato, S.; Bierbaum, V. M.; Lineberger, W. C.; Ellison, G. B.; Okumura, M. *J. Am. Chem. Soc.* **2001**, *123*, 9585.
(21) Zalyubovsky, S. J.; Wang, D.; Miller, T. A. *Chem. Phys. Lett.* **2001**, *335*, 298.
(22) Atkinson, R. *J. Phys. Chem. Ref. Data* **1997**, *26*, 215.
(23) Atkinson, R. *Int. J. Chem. Kinet.* **1987**, *19*, 799.
(24) Atkinson, R.; Carter, W. P. L.; Winer, A. M. *J. Phys. Chem.* **1983**, *87*, 2012.
(25) Sander, S. P.; Watson, R. T. *J. Phys. Chem.* **1980**, *84*, 1664.
(26) Ravishankara, A. R.; Eisele, F. L.; Kreutter, N. M.; Wine, P. H. *J. Phys. Chem.* **1981**, *74*, 2267.
(27) Simonaitis, R.; Heicklen, J. *J. Phys. Chem.* **1981**, *85*, 2946.
(28) Plumb, I. C.; Ryan, K. R.; Steven, J. R.; Mulcahy, M. F. R. *J. Phys. Chem.* **1981**, *85*, 3136.
(29) Plumb, I. C.; Ryan, K. R.; Steven, J. R.; Mulcahy, M. F. R. *Int. J. Chem. Kinet.* **1982**, *14*, 183.
(30) Cox, R. A.; Tyndall, G. S. *J. Chem. Soc., Faraday Trans.* **1980**, *76*, 153.
(31) Zellner, R.; Fritz, B.; Lorenz, K. *J. Atmos. Chem.* **1986**, *4*, 241.
(32) Kenner, R. D.; Ryan, K. R.; Plumb, I. C. *Geophys. Res. Lett.* **1993**, *20*, 1571.
(33) Sehested, J.; Nielsen, O. J.; Wallington, T. J. *Chem. Phys. Lett.* **1993**, *213*, 457.
(34) Daele, V.; Ray, A.; Vassalli, I.; Poulet, G.; LeBras, G. *Int. J. Chem. Kinet.* **1995**, *27*, 1121.
(35) Adachi, H.; Basco, N.; James, D. G. *Int. J. Chem. Kinet.* **1979**, *11*, 1211.
(36) Ranschaert, D. L.; Schneider, N. J.; Elrod, M. J. *J. Phys. Chem. A* **2000**, *104*, 5758.
(37) Elfers, G.; Zabel, F.; Becker, K. H. *Chem. Phys. Lett.* **1990**, *168*, 14.
(38) Adachi, H.; Basco, N. *Chem. Phys. Lett.* **1979**, *67*, 324.
(39) Ravishankara, A. R.; Eisele, F. L.; Wine, P. H. *J. Chem. Phys.* **1980**, *73*, 3743.
(40) Cox, R. A.; Tyndall, G. S. *Chem. Phys. Lett.* **1979**, *65*, 357.
(41) Jenkin, M. E.; Boyd, A. A.; Lesclaux, R. *J. Atmos. Chem.* **1998**, *29*, 267.
(42) McAdam, K.; Veyret, B.; Lesclaux, R. *Chem. Phys. Lett.* **1987**, *133*, 39.
(43) Kurylo, M. J.; Dagaut, P.; Wallington, T. J.; Newman, S. M. *Chem. Phys. Lett.* **1987**, *139*, 513.
(44) Dagaut, P.; Kurylo, M. J.; Wallington, T. J. *J. Phys. Chem.* **1988**, *92*, 3833.
(45) Lightfoot, P. D.; Veyret, B.; Lesclaux, R. *J. Phys. Chem.* **1990**, *94*, 708.
(46) Villalta, P. W.; Huey, G.; Howard, C. J. *J. Phys. Chem.* **1995**, *99*, 12829.
(47) Lightfoot, P. D.; Roussel, P.; Caralp, F.; Lesclaux, R. *J. Chem. Soc., Faraday Trans.* **1991**, *87*, 3213.
(48) Cattell, F. C.; Cavanagh, J.; Cox, R. A.; Jenkin, M. E. *J. Chem. Soc., Faraday Trans. 2* **1986**, *82*, 1999.
(49) Fenter, F. F.; Catoire, V.; Lesclaux, R.; Lightfoot, P. D. *J. Phys. Chem.* **1993**, *97*, 3530.
(50) Maricq, M. M.; Szente, J. *J. Phys. Chem.* **1994**, *98*, 2078.
(51) Crawford, M. A.; Wallington, T. J.; Szente, J. J.; Maricq, M. M.; Francisco, J. S. *J. Phys. Chem. A* **1999**, *103*, 365.
(52) Wallington, T. J. *J. Chem. Soc., Faraday Trans.* **1991**, *87*, 2379.
(53) Wallington, T. J.; Japar, S. M. *Chem. Phys. Lett.* **1990**, *16*, 495.
(54) Jenkin, M. E.; Murrells, T. P.; Shalliker, S. J.; Hayman, G. D. *J. Chem. Soc., Faraday Trans.* **1993**, *89*, 433.
(55) Jenkin, M. E.; Hayman, G. D. *J. Chem. Soc., Faraday Trans.* **1995**, *91*, 1911.
(56) Nielsen, O. J.; Sehested, J.; Langer, S.; Ljungstrom, E.; Wangberg, I. *Chem. Phys. Lett.* **1995**, *238*, 359.
(57) Barnes, I.; Becker, K. H.; Ruppert, L. *Chem. Phys. Lett.* **1993**, *203*, 295.
(58) Villenave, E.; Lesclaux, R.; Seefeld, S.; Stockwell, W. R. *J. Geophys. Res.* **1998**, *103*, 25273.
(59) Rowley, D. M.; Lightfoot, P. D.; Lesclaux, R.; Wallington, T. J. *J. Chem. Soc., Faraday Trans.* **1991**, *87*, 3221.
(60) Henon, E.; Bohr, F.; Chakir, A.; Brion, J. *Chem. Phys. Lett.* **1997**, *264*, 557.
(61) Boyd, A. A.; Noziere, B.; Lesclaux, R. *J. Chem. Soc., Faraday Trans.* **1996**, *92*, 201.
(62) Catoire, V.; Lesclaux, R.; Schneider, W. F.; Wallington, T. J. *J. Phys. Chem.* **1996**, *100*, 14356.
(63) Crawford, M. A.; Szente, J. J.; Maricq, M. M.; Francisco, J. S. *J. Phys. Chem. A* **1997**, *101*, 5337.
(64) Moortgat, G. K.; Veyret, B.; Lesclaux, R. *Chem. Phys. Lett.* **1989**, *160*, 443.
(65) Noziere, B.; Lesclaux, R.; Hurley, M. D.; Dearth, M. A.; Wallington, T. J. *J. Phys. Chem.* **1994**, *98*, 2864.
(66) Rowley, D. M.; Lesclaux, R.; Lightfoot, P. D.; Hughes, K.; Hurley, M. D.; Rudy, S.; Wallington, T. J. *J. Phys. Chem.* **1992**, *96*, 7043.
(67) Rowley, D. M.; Lesclaux, R.; Lightfoot, P. D.; Noziere, B.; Wallington, T. J.; Hurley, M. D. *J. Phys. Chem.* **1992**, *96*, 4889.
(68) Sehested, J.; Mogelberg, T.; Fagerstrom, K.; Mahmoud, G.; Wallington, T. J. *Int. J. Chem. Kinet.* **1997**, *29*, 673.
(69) Villenave, E.; Lesclaux, R. *J. Phys. Chem. A* **2001**, *104*, 9933.
(70) Tuazon, E. C.; Aschmann, S. M.; Atkinson, R.; Carter, W. P. L. *J. Phys. Chem. A* **1998**, *102*, 2316.
(71) Kwok, E. S. C.; Arey, J.; Atkinson, R. *J. Phys. Chem.* **1996**, *100*, 214.
(72) Aschmann, S. M.; Chew, A. A.; Arey, J.; Atkinson, R. *J. Phys. Chem. A* **1997**, *101*, 8042.
(73) Bauer, D.; Crowley, J. N.; Moortgat, G. K. *J. Photochem. Photobiol. A: Chem.* **1992**, *65*, 329.
(74) Biggs, P.; Canosa-Mas, C. E.; Fracheboud, J.-M.; Percival, C. J.; Wayne, R. P.; Shallcross, D. E. *J. Chem. Soc., Faraday Trans.* **1997**, *93*, 379.
(75) Maricq, M. M.; Szente, J. J. *J. Phys. Chem. A* **2000**, *104*, 7239.
(76) Maricq, M. M.; Szente, J. J. *J. Phys. Chem.* **1996**, *100*, 12374.
(77) Scholtens, K. W.; Messer, B. M.; Cappa, C. D.; Elrod, M. J. *J. Phys. Chem. A* **1999**, *103*, 4378.
(78) Stevens, P.; L'Esperance, D.; Martin, G. *Int. J. Chem. Kinet.* **1999**, *31*, 637.
(79) Villenave, E.; Morozov, I.; Lesclaux, R. *J. Phys. Chem. A* **2000**, *104*, 9933.
(80) Villalta, P. W.; Howard, C. J. *J. Phys. Chem.* **1996**, *100*, 13624.
(81) Villalta, P. W.; Huey, G.; Howard, C. J. *J. Phys. Chem.* **1995**, *99*, 12829.
(82) Romanini, D.; Kachanov, A. A.; Sadeghi, N.; Stoeckel, F. *Chem. Phys. Lett.* **1997**, *264*, 316.
(83) He, Y.; Hippler, M.; Quack, M. *Chem. Phys. Lett.* **1998**, *289*, 527.
(84) Paldus, B. A.; Harris, J. S., Jr.; Martin, J.; Xie, J.; Zare, R. N. *J. Appl. Phys.* **1997**, *82*, 3199.
(85) Yu, T.; Lin, M. C. *J. Am. Chem. Soc.* **1993**, *115*, 4371.
(86) O'Keefe, A.; Deacon, D. A. G. *Rev. Sci. Instrum.* **1988**, *59*, 2544.
(87) Pipino, A. C. R.; Hudgens, J. W.; Huie, R. E. *Chem. Phys. Lett.* **1997**, *280*, 104.
(88) Pipino, A. C. R. *Proc. SPIE-Int. Soc. Opt. Eng.* **1999**, *3535*, 57.
(89) Engeln, R.; Letourneur, K. G. Y.; Boogaarts, M. G. H.; Van de Sanden, M. C. M.; Schram, D. C. *Chem. Phys. Lett.* **1999**, *310*, 405.
(90) Scherer, J. J.; Aniolek, K. W.; Rakestraw, D. J. *J. Chem. Phys.* **1997**, *107*, 6196.

(91) Mercier, X.; Therssen, E.; Pauwels, J. F.; Desgroux, P. *Combust. Flame* **2001**, *124*, 656.
(92) Mercier, X.; Pillier, L.; Pauwels, J.-F.; Desgroux, P. *Comptes Rendus l'Acad. Sci., Ser. IV: Phys., Astrophys.* **2001**, *2*, 965.
(93) Luque, J.; Jeffries, J. B.; Smith, G. P.; Crosley, D. R. *Appl. Phys. B − Lasers O* **2001**, *73*, 731.
(94) Booth, J. P.; Cunge, G.; Biennier, L.; Romanini, D.; Kachanov, A. *Chem. Phys. Lett.* **2000**, *317*, 631.
(95) Derzy, I.; Lozovsky, V. A.; Ditzian, N.; Rahinov, I.; Cheskis, S. *Proc. Combust. Inst.* **2000**, *28*, 1741.
(96) Lozovsky, V. A.; Derzy, I.; Cheskis, S. *Symp. (Int.) Combust., [Proc.]* **1998**, *27*, 445.
(97) Cheskis, S. *Prog. Energy Combust. Sci.* **1999**, *25*, 233.
(98) Kessels, W. M. M.; Hoefnagels, J. P. M.; Boogaarts, M. G. H.; Schram, D. C.; van de Sanden, M. C. M. *J. Appl. Phys.* **2001**, *89*, 2065.
(99) Boogaarts, M. G. H.; Bocker, P. J.; Kessels, W. M. M.; Schram, D. C.; van de Sanden, M. C. M. *Chem. Phys. Lett.* **2000**, *326*, 400.
(100) Evertsen, R.; Stolk, R. L.; Ter Meulen, J. J. *Combust. Sci. Technol.* **2000**, *157*, 341.
(101) McIlroy, A. *Isr. J. Chem.* **1999**, *39*, 55.
(102) Thoman, J. W., Jr.; McIlroy, A. *J. Phys. Chem. A* **2000**, *104*, 4953.
(103) Xie, J.; Paldus, B. A.; Wahl, E. H.; Martin, J.; Owano, T. G.; Kruger, C. H.; Harris, J. S.; Zare, R. N. *Chem. Phys. Lett.* **1998**, *284*, 387.
(104) Sappey, A. D.; Hill, E. S.; Settersten, T.; Linne, M. A. *Opt. Lett.* **1998**, *23*, 954.
(105) Brown, S. S.; Stark, H.; Ciciora, S. J.; Ravishankara, A. R. *Geophys. Res. Lett.* **2001**, *28*, 3227.
(106) Kleine, D.; Murtz, M.; Lauterbach, J.; Dahnke, H.; Urban, W.; Hering, P.; Kleinermanns, K. *Isr. J. Chem.* **2001**, *41*, 111.
(107) Smith, J. D.; Atkinson, D. B. *Analyst* **2001**, *126*, 1216.
(108) Thompson, J. E.; Smith, B. W.; Winefordner, J. D. *Anal. Chem.* **2002**, *74*, 1962.
(109) Zhang, J.; Wang, L. *Preprints of Extended Abstracts presented at the ACS National Meeting*; American Chemical Society, Division of Environmental Chemistry; American Chemical Society: Washington, DC, 2002; Vol. 42, p 657.
(110) Atkinson, D. B.; Hudgens, J. W. *J. Phys. Chem. A* **1997**, *101*, 3901.
(111) Brown, S. S.; Ravishankara, A. R.; Stark, H. *J. Phys. Chem. A* **2000**, *104*, 8600.
(112) Park, J.; Lin, M. C. *ACS Symp. Ser.* **1999**, *720*, 196.
(113) Ninomiya, Y.; Goto, M.; Hashimoto, S.; Kawasaki, M.; Wallington, T. J. *Int. J. Chem. Kinet.* **2001**, *33*, 130.
(114) *Cavity-Ringdown Spectroscopy An Ultratrace-Absorption Measurement Technique*; Busch, K. W., Busch, M. A., Eds.; American Chemical Society (distributed by Oxford University Press): Washington, DC, 1999; Vol. 720.
(115) Berden, G.; Peeters, R.; Meijer, G. *Int. Rev. Phys. Chem.* **2000**, *19*, 565.
(116) Scherer, J. J.; Paul, J. B.; Saykally, R. J. *Chem. Rev.* **1997**, *97*, 25.
(117) Wheeler, M. D.; Newman, S. M.; Orr-Ewing, A. J.; Ashfold, M. N. R. *J. Chem. Soc., Faraday Trans.* **1998**, *94*, 337.
(118) Paldus, B. A. *From pulsed to continuous wave cavity ring-down spectroscopy*; Stanford University, Stanford, CA, 1998.
(119) Paldus, B. A.; Harb, C. C.; Spence, T. G.; Wilke, B.; Xie, J.; Harris, J. S.; Zare, R. N. *J. Appl. Phys.* **1998**, *83*, 3991.
(120) Romanini, D.; Kachanov, A. A.; Stoeckel, F. *Chem. Phys. Lett.* **1997**, *270*, 538.
(121) Schulz, K. J.; Simpson, W. R. *Chem. Phys. Lett.* **1998**, *297*, 523.
(122) Hodges, J. T.; Looney, J. P.; van Zee, R. D. *Appl. Opt.* **1996**, *35*, 4112.
(123) Braun, W.; Herron, J. T.; Kahaner, D. K. *Int. J. Chem. Kinet.* **1988**, *20*, 51.
(124) Zalicki, P.; Zare, R. N. *J. Chem. Phys.* **1995**, *102*, 2708.
(125) Scherer, J. J.; Paul, J. B.; O'Keefe, A.; Saykally, R. J. *Chem. Rev.* **1997**, *97*, 25.
(126) Atkinson, D. B.; Hudgens, J. W. *J. Phys. Chem. A* **1999**, *103*, 4242.
(127) DeMore, W. B.; Sander, S. P.; Golden, D. M.; Hampson, R. F.; Kurylo, M. J.; Howard, C. J.; Ravishankara, A. R.; Kolb, C. E.; Molina, M. J. *Chemical Kinetics and Photochemical Data for Use in Stratospheric Modeling*; Jet Propulsion Laboratory, California Institute of Technology: Pasadena, CA, 1997.